

CM² MAGAZINE



第 72 期



南方科技大学海洋磁学中心主编

https://cm².sustech.edu.cn/

创刊词

海洋是生命的摇篮，是文明的纽带。地球上最早的生命诞生于海洋，海洋里的生命最终进化成了人类，人类的文化融合又通过海洋得以实现。人因海而兴。

人类对海洋的探索从未停止。从远古时代美丽的神话传说，到麦哲伦的全球航行，再到现代对大洋的科学钻探计划，海洋逐渐从人类敬畏崇拜幻想的精神寄托演变成可以开发利用与科学研究的客观存在。其中，上个世纪与太空探索同步发展的大洋科学钻探计划将人类对海洋的认知推向了崭新的纬度：深海（deep sea）与深时（deep time）。大洋钻探计划让人类知道，奔流不息的大海之下，埋藏的却是亿万年的地球历史。它们记录了地球板块的运动，从而使板块构造学说得到证实；它们记录了地球环境的演变，从而让古海洋学方兴未艾。

在探索海洋的悠久历史中，从大航海时代的导航，到大洋钻探计划中不可或缺的磁性地层学，磁学发挥了不可替代的作用。这不是偶然，因为从微观到宏观，磁性是最基本的物理属性之一，可以说，万物皆有磁性。基于课题组的学科背景和对海洋的理解，我们对海洋的探索以磁学为主要手段，海洋磁学中心因此而生。

海洋磁学中心，简称 CM^2 ，一为其全名“Centre for Marine Magnetism”的缩写，另者恰与爱因斯坦著名的质能方程 $E = MC^2$ 对称，借以表达我们对科学巨匠的敬仰和对科学的不懈追求。

然而科学从来不是单打独斗的产物。我们以磁学为研究海洋的主攻利器，但绝不仅限于磁学。凡与磁学相关的领域均是我们关注的重点。为了跟踪反映国内外地球科学特别是与磁学有关的地球科学领域的最新研究进展，海洋磁学中心特地主办 CM^2 Magazine，以期与各位地球科学工作者相互交流学习、合作共进！

“海洋孕育了生命，联通了世界，促进了发展”。21世纪是海洋科学的时代，由陆向海，让我们携手迈进中国海洋科学的黄金时代。

目 录

一、研究进展.....	1
1. 西非板块在元古代 Nuna 超大陆中位置的新约束.....	1
2. 印度-亚洲大陆碰撞及大印度北向延伸尺度的古地磁学约束.....	5
二、文献进展.....	8
1. 沉积古 DNA 记录揭示由于气候变暖导致高山栖息地的减少会直接威胁青藏高原植物多样性.....	8
2. 早太古代碳酸盐与洋壳俯冲的钙同位素证据.....	11
3. 冰川-全新世湖泊和陆地环境气候驱动的转变：来自南极东部 Mochou 湖岩石磁学和地球化学证据.....	13
4. 东南极洲与冈瓦纳曾经相邻的磁场联系.....	17
5. 上新世-更新世过渡时期东赤道太平洋稳定的生物生产力(3.35-2.0 Ma).19	
6. 极弱地磁场的时期延长：埃迪卡拉纪 Grenville(SE Canada)岩墙的古强度结果.....	22
7. 末次冰期地磁偶极子场变化—分离气候和生产速率信号后的格陵兰冰芯宇宙核素记录.....	25
8. 由希克苏鲁伯撞击触发的显著而短暂的海洋生产力爆发.....	28

一、研究进展

1. 西非板块在元古代 Nuna 超大陆中位置的新约束

超大陆旋回对地球生命与环境演化有着深刻意义。元古代 Nuna 超大陆可能是地球历史上最早的一个超大陆，对其研究有助于我们认识早期地球板块的活动模式，以及超大陆拼合、裂解的过程及其影响。目前人们对于 Nuna 超大陆的构型仍有诸多疑问。古地磁是进行板块重建的最有效手段之一。近年来，随着古地磁数据不断丰富，劳伦，波罗的，西伯利亚，华北，澳大利亚等板块在 Nuna 超大陆中的位置日渐清晰。但其他板块仍缺乏有效的古地理约束，西非板块就是其中之一。在此前的很多 Nuna 超大陆模型中，西非南部被放置于亚马逊东北侧，这与两板块在冈瓦纳大陆的相对位置一致。但支持这种连接方式的证据并不充足，也缺乏古地磁数据的约束。

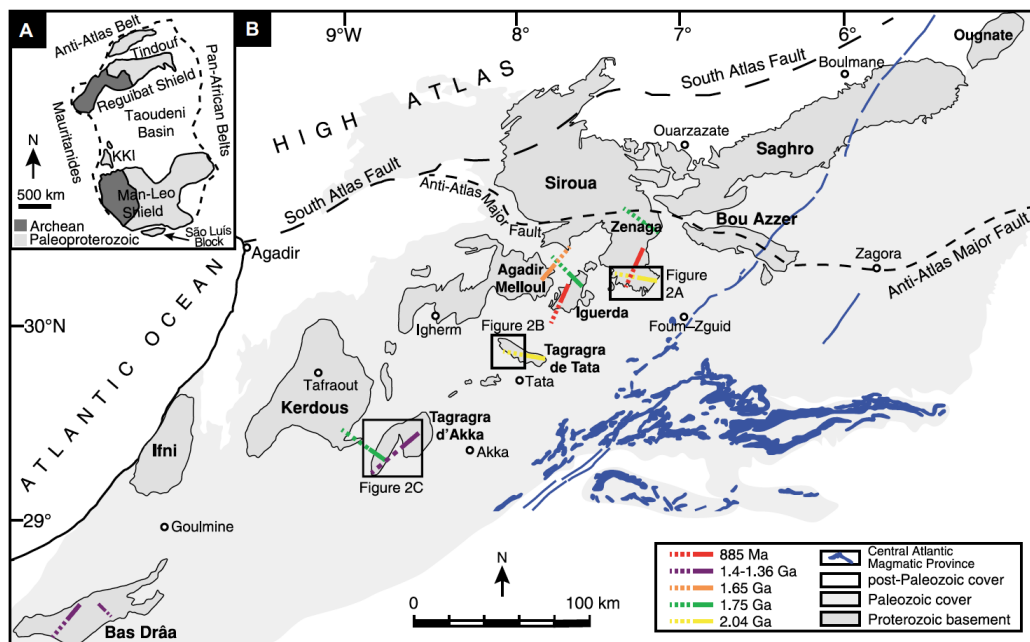


图 1 (A) 西非地质简图。(B) 摩洛哥 Anti-Atlas Belt 地区基性岩墙的年龄及走向分布。

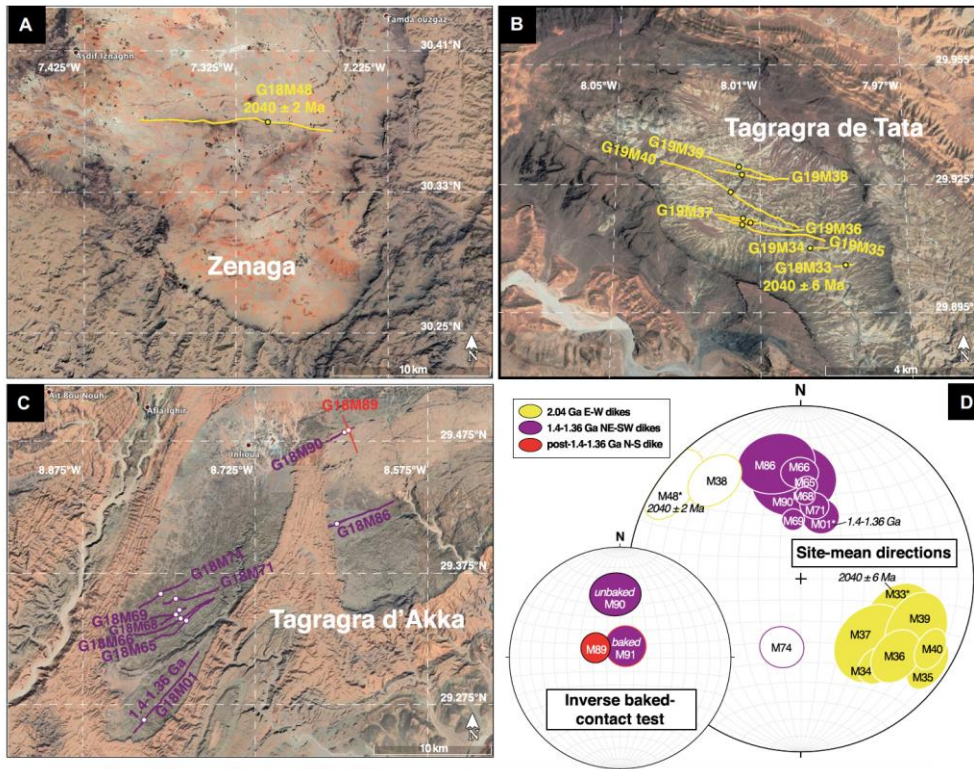


图 2 (A-C) 研究区域的卫星图以及采样岩墙分布。(D) 岩墙的古地磁结果图。

本文对西非板块摩洛哥的 Anti-Atlas Belt 地区的元古代基性岩墙开展了古地磁学和 U-Pb 年代学研究 (图 1, 2), 得到了两个可靠的古地磁极, 一个约为 20 亿年, 另一个约为 14 亿年。通过与其他板块的古地磁数据进行对比, 本文尝试对西非板块在 Nuna 超大陆中位置提供新的约束。在比较了西非与亚马逊 21-20 亿年间的古地磁视极移曲线后, 我们第一次提出了西非北部与亚马逊东北部相连接的模式 (图 3A)。在 Nuna 超大陆中, 古地磁数据同样支持西非与亚马逊这种新的连接方式 (图 3B, C)。此外, 地质证据和大火成岩省的分布也与我们的新模型相符 (图 4)。

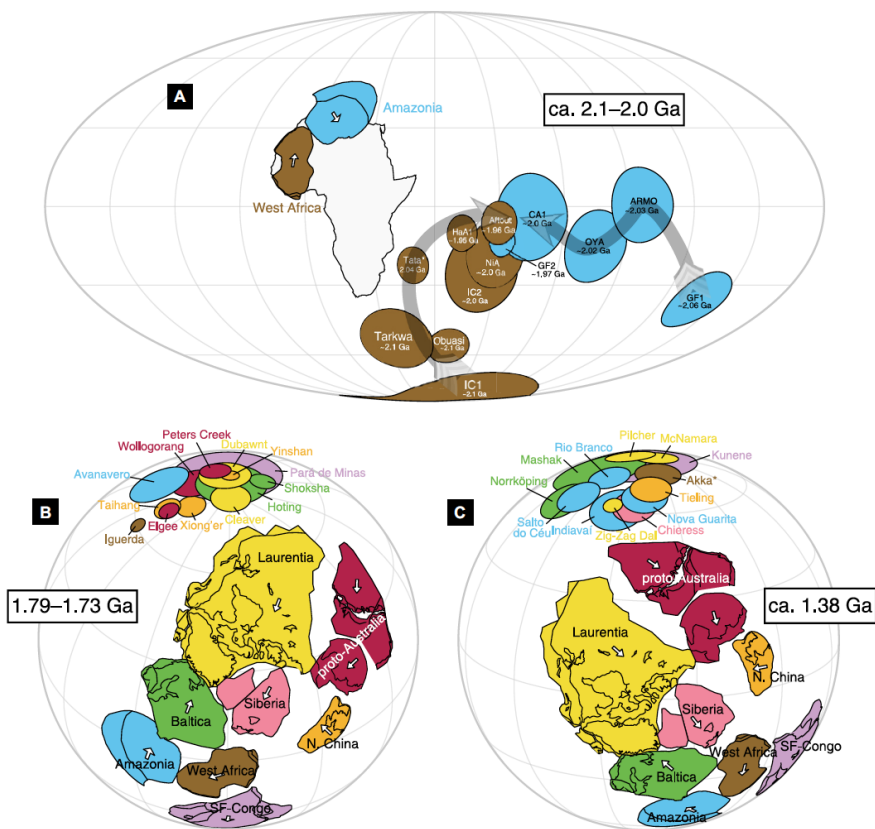


图3 板块重建图。(A) 21-20 亿年西非与亚马逊古地磁视极移曲线指示两板块在 20 亿年左右聚合。(B-C) Nuna 超大陆重建图，及 17 亿和 14 亿年左右 Nuna 超大陆主要板块的古地磁数据对比。

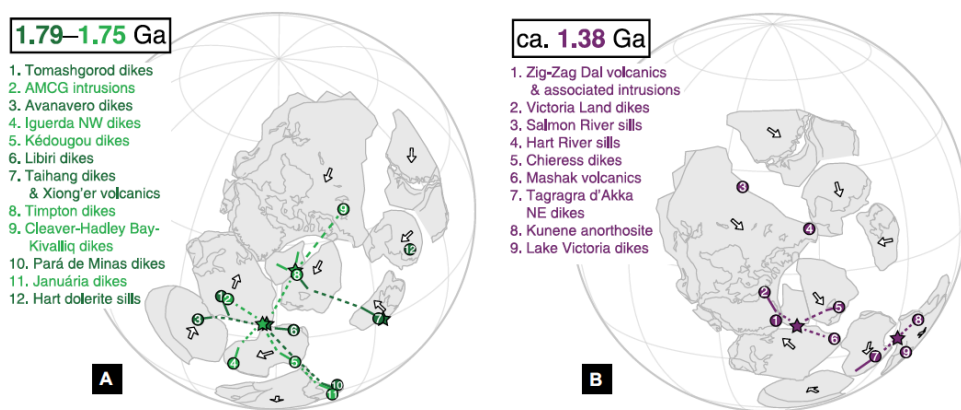


图4 全球大火成岩省在新 Nuna 超大陆重建模型上的分布。星号表示地幔柱的可能位置，直线表示岩墙群的走向，虚线表示侵入体间的可能连接方式。

本文的结果对理解板块间相互运动，以及超大陆旋回有着一定的启发意义。新的西非与亚马逊连接方式意味着在 Nuna 超大陆裂解至冈瓦纳大陆聚合期间的约 8 亿年间，西非和亚马逊的相对位置变化了约 180 度。这种大尺度的板块间相对运动之前未被重视，但在地质历史上并非罕见。例如，西伯利亚和波罗的在埃迪卡拉和二叠纪这段时间中相对旋转了约 180 度；在 Rodinia 超大陆形成过程中，亚马逊相对劳伦旋转了约 180 度；华北和澳大利亚的相对位置在早古生代与在 Nuna 超大陆中相比也变化了约 180 度等。这种大尺度的相对旋转并非由板块的原地旋转完成，而更可能是一系列长时间多样的板块运动（如聚合，分裂，走滑）积累所致。除此之外，此前一些学者认为 Nuna 超大陆的裂解并不彻底，导致 Rodinia 超大陆与 Nuna 超大陆构型非常相似，其可能是元古代 18-8 亿年间地球演化过程相对“无聊”的原因。但近几年来人们逐渐意识到，Nuna 超大陆，尤其是其中劳伦东侧的板块位置在形成 Rodinia 超大陆过程中似乎发生了大规模的改造，Nuna 超大陆的裂解与 Rodinia 超大陆的聚合过程很可能比之前认为的复杂很多。对于 Nuna-Rodinia 这一超大陆旋回认识的完善以及其对地球演化影响的理解需要未来更多高质量的古地磁研究及其他相关地质学研究。

该成果近期发表于 Gong, Z., Evans, D. A. D., Youbi, N., Ait Lahna, A., Söderlund, U., Ait Malek, M., Wen, B., Jing, X. Q., Ding, J. K., Boumehdi, M. & Ernst, R. E. (in press). Reorienting the West African craton in Paleoproterozoic-Mesoproterozoic supercontinent Nuna: *Geology*, v. 49, p. XXX. <https://doi.org/10.1130/G48855.1>.



第一作者简介：龚政，现为耶鲁大学地球与行星科学系博士研究生。研究方向主要为前寒武板块构造，古地磁学及旋回地层学。

2. 印度-亚洲大陆碰撞及大印度北向延伸尺度的古地磁学约束

印度-亚洲大陆的碰撞及后续持续挤压不仅形成了世界上海拔最高的高原——青藏高原,而且对全球古地理、古环境、古气候以及生命演化产生了重要的影响。正确认识印度-亚洲大陆何时、何地并且如何发生碰撞,对理解青藏高原大地构造演化和古气候演变至关重要(Hu et al., 2016)。尽管前人在雅鲁藏布江缝合带及其两侧地体开展了大量的地质与地球物理研究,但不同学者采用不同方法获得的印度-亚洲大陆的碰撞时限从~70 Ma(Yin and Harrison, 2000)到~34 Ma(Aitchison et al., 2007)不等。如此大的差异与不同的印度-亚洲大陆碰撞过程及不同的大印度北向延伸尺度密切相关。

对于印度-亚洲大陆碰撞过程主要包含单阶段碰撞模型和两阶段碰撞模型两大类。其中单阶段碰撞模型主要包括大印度陆陆碰撞模型(Ingalls et al., 2016)和小印度陆陆碰撞模型(Yang et al., 2019)。而两阶段碰撞模型主要包括陆弧+陆陆模型(Aitchison et al., 2007)、弧陆+陆陆模型(Pusok and Stegman, 2020)、大印度盆地+双陆陆模型(van Hinsbergen et al., 2012)及北印度海+双陆陆模型(Yuan et al., 2021)。对于大印度北向延伸尺度,从没有明显的北向延伸到北向延伸超过其现今北部边界约3400公里(DeCelles et al., 2002; Ali and Aitchison, 2005; Yi et al., 2011; van Hinsbergen et al., 2019; Meng et al., 2020)。

为更好限定印度-亚洲大陆碰撞及大印度北向延伸尺度,中国地质大学(北京)边伟伟博士(现为中国科学院地质与地球物理研究所博士后)、杨天水教授、彭文骁博士研究生、王锁博士研究生、高峰硕士、张世红教授、吴怀春教授、李海燕副研究员、曹丽婉讲师、江湑副教授及中国地质大学(武汉)王华沛教授共同合作,对特提斯喜马拉雅堆纳-岗巴地区遮普惹组灰岩(图1)开展了详细的构造古地磁学、碎屑锆石U-Pb年代学、岩石磁学、岩相学及磁性地层学研究,获得了由精确年代学和褶皱及倒转检验约束的可靠的古地磁结果,结合拉萨地块、特提斯喜马拉雅和印度克拉通白垩纪至始新世已有的可靠的古地磁结果,获得以下认识:

1. 特提斯喜马拉雅在~51–49.5 Ma 位于 $15.2^{\circ} \pm 2.6^{\circ}\text{N}$;
2. 特提斯喜马拉雅和印度克拉通之间有~900–1140 km 南北向地壳缩短(图

2);

3. 印度-亚洲大陆碰撞不晚于~51–49.5 Ma (图 2)。

该成果不仅准确的厘定了特提斯喜马拉雅堆纳-岗巴采样区遮普惹组灰岩的形成时代及其形成时的古地理位置，而且为印度-亚洲大陆碰撞及大印度北向延伸尺度提供了可靠的古地磁学约束，同时为探究青藏高原大地构造演化及古气候演变提供了新的依据。

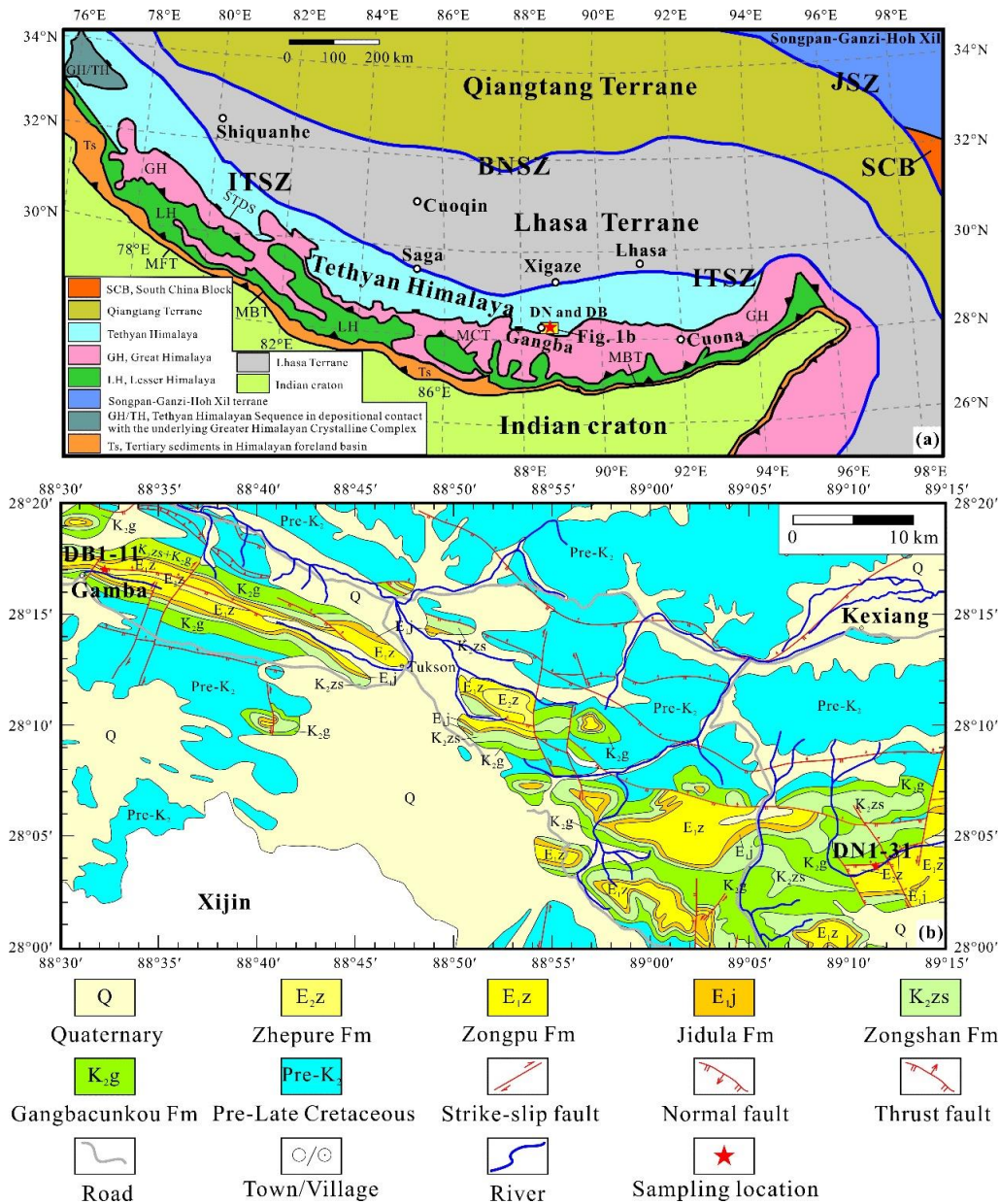


图 1 喜马拉雅及其邻区大地构造简图 (a) 和堆纳-岗巴地区采样剖面示意图 (b)

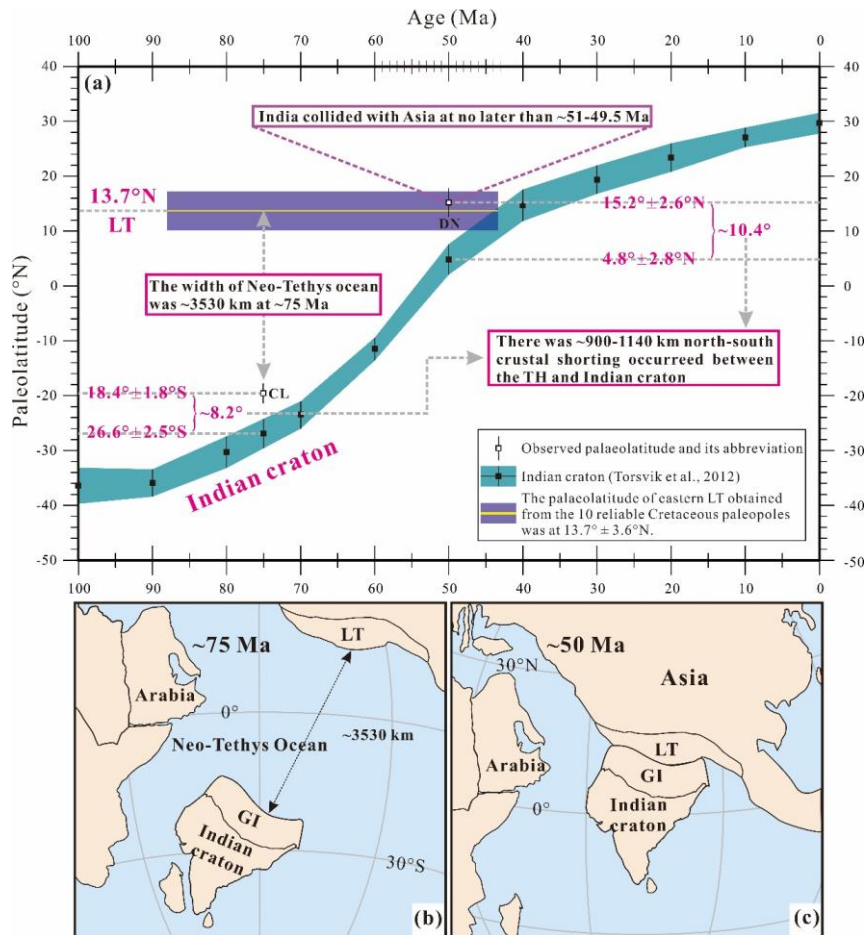


图 2 特提斯喜马拉雅、拉萨地块和印度克拉通古纬度演化图

该成果近期发表于Journal of Geophysical Research: Solid Earth上。Bian, W., Yang, T., Peng, W., Wang, S., Gao, F., Zhang, S., Wu H., Li H., Cao L., Jiang T., and Wang H. (2021). Paleomagnetic constraints on the India–Asia collision and the size of Greater India. Journal of Geophysical Research: Solid Earth, 126, e2021JB021965.

<https://doi.org/10.1029/2021JB021965>



第一作者简介：边伟伟，现为中国科学院地质与地球物理研究所博士后，研究方向主要为构造古地磁学。

二、文献进展

1. 沉积古 DNA 记录揭示由于气候变暖导致高山栖息地的减少会直接威胁青藏高原植物多样性

翻译人：仲义 zhongy@sustech.edu.cn



Liu S S, Kruse S, Scherler D, et al. *Sedimentary ancient DNA reveals a threat of warming-induced alpine habitat loss to Tibetan Plateau plant diversity* [J]. *Nature Communications*, 2021, 12(1):2995.

<https://doi.org/10.1038/s41467-021-22986-4>

摘要: 在世界范围内沿海拔梯度研究会经常发现在海拔梯度居中地区森林植物物种的丰富度最高。因此，在与气候变暖相关的林线上升过程中，较高海拔地区的植物多样性可能会增加。本文采用时间序列的方法，从青藏高原东南部近 1.8 万年的沉积古 DNA 中推断了过去植物类群的丰富程度。结果发现，植物丰富度的峰值出现在冰川消退后的冷期（14-10 ka），该时期包含了广泛和多样性的高山植被环境；紧接着在早-中全新世暖期（10-3.6 ka），森林扩张，植物的丰富度开始下降。3.6 ka 以来放牧对植物类群丰富度的促进作用较弱。基于这些推断的相关性，我们的模拟结果显示，在接下来的几个世纪里，由于与气候变暖相关的高山环境的缺失，植物类群的丰富度将大幅度下降。因此，对于青藏高原地区生物多样性保护研究应该更多借鉴与参考古生态学研究的证据。

ABSTRACT: Studies along elevational gradients worldwide usually find the highest plant taxa richness in mid-elevation forest belts. Hence, an increase in upper elevation diversity is expected in the course of warming-related treeline rise. Here, we use a time-series approach to infer past taxa richness from sedimentary ancient DNA from the south-eastern Tibetan Plateau over the last ~18,000 years. We find the highest total plant taxa richness during the cool phase after glacier retreat when the area contained

extensive and diverse alpine habitats (14–10 ka); followed by a decline when forests expanded during the warm early- to mid-Holocene (10–3.6 ka). Livestock grazing since 3.6 ka promoted plant taxa richness only weakly. Based on these inferred dependencies, our simulation yields a substantive decrease in plant taxa richness in response to warming-related alpine habitat loss over the next centuries. Accordingly, efforts of Tibetan biodiversity conservation should include conclusions from palaeoecological evidence.

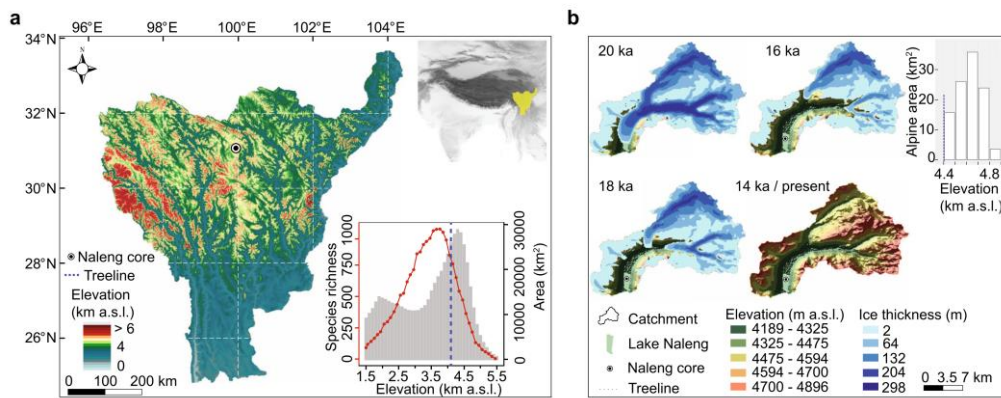


Figure 1. The Naleng lacustrine core was recovered from the centre of Lake Naleng (black bullet point), in the Hengduan Mountains, a designated biodiversity hotspot in East Asia. a Location of the Hengduan Mountains on the south-eastern Tibetan Plateau, China (top-right inset, yellow fill). Area-elevation relationship (grey bars), elevational species richness distribution (red dotted line), and forest zone (blue dashed line) are shown in the lower-right inset. b Lake Naleng catchment area is 128 km². The simulation of the glacier extent (Methods) indicates that the Lake Naleng catchment became ice-free by about 14 ka. The extent of alpine area per 100-m elevation is shown as white bars.

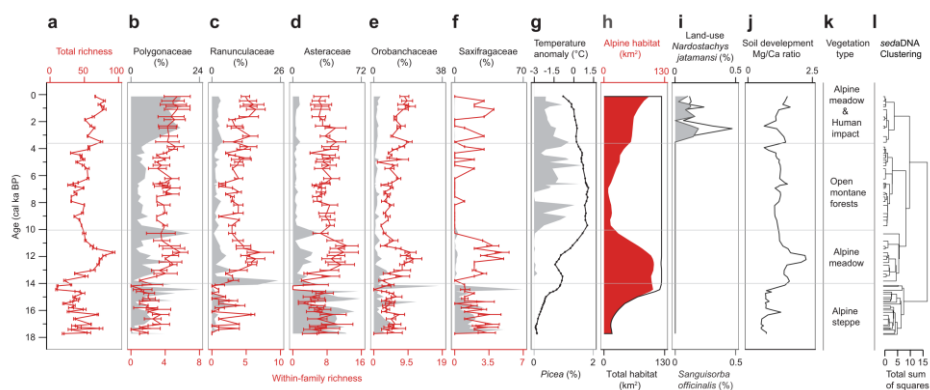


Figure 2. Long-term history of plant sedaDNA recorded in Lake Naleng compared with time-series data.

a Total plant richness (red line; $n = 138$ PCR replicates of 71 lake-sediments, bars indicate 95% confidence intervals). b–f Comparison of sedimentary ancient DNA abundance (in %, grey polygon) of the most common alpine plant families with corresponding within-family plant richness (red line; $n = 138$ PCR replicates of 71 lake-sediments, bars indicate 95% confidence intervals) for Polygonaceae, Ranunculaceae, Asteraceae, Orobanchaceae, and Saxifragaceae. g The Northern Hemisphere (30° – 90° N) temperature anomaly record since last deglaciation based on multiple proxies (black line with points, Methods) and percentage of *Picea* sedaDNA (grey polygon). h Alpine habitat area (red polygon) within the Lake Naleng catchment is the sum of pixels above the treeline (4400 m a.s.l.) based on simulated total habitat area (black outline, Methods). i sedaDNA indicators of traditional land-use including *Sanguisorba officinalis* (grey polygon) and *Nardostachys jatamansi* (black line). j The Mg/Ca ratio of Lake Naleng indicates the soil development within the lake catchment. k vegetation types inferred from the pollen record and sedaDNA record. l Zonation (horizontal grey lines) according to a stratigraphically constrained cluster analysis (CONISS) based on relative read abundance. Data are presented as mean \pm 95% confidence interval (error bars) in a–f. Source data are provided with this paper.

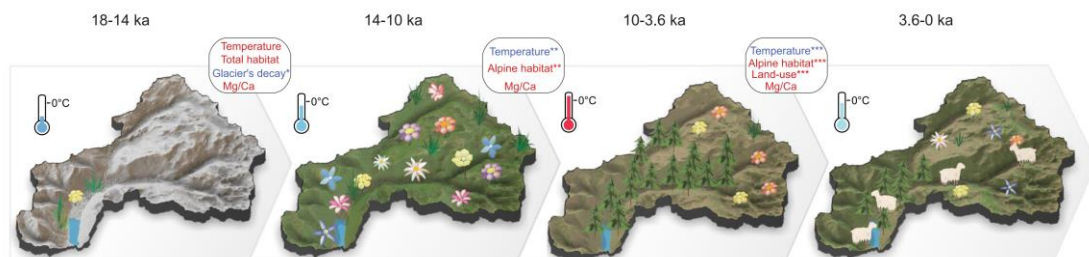


Figure 3. Visualization of total plant taxa richness and effects of abiotic factors on plant richness across four time-intervals. We calculated the statistical relationship between total plant richness and predictor variables (rounded rectangle) between consecutive periods of time (Methods). Alpha significance codes of Spearman correlation are ***0.0005, **0.01, and *0.025 according to adjusted degrees of freedom. The mean annual temperature anomaly is indicated by the thermometer. Positive and negative correlation is marked in red and blue font, respectively. The catchment sketches illustrate that disturbance in the glaciated landscape was likely of importance during the deglaciation period. Our results indicate that once the catchment became icefree, alpine habitat extent is the main driver of total plant richness while land-use is only of secondary importance during the late Holocene. From the switch in correlation sign, we assume that temperature is likely not a direct driver of richness change.

2. 早太古代碳酸盐与洋壳俯冲的钙同位素证据

翻译人: 冯婉仪 fengwy@sustech.edu.cn



Antonelli M A, Kendrick J, Yakymchuk C, et al. *Calcium isotope evidence for early Archaean carbonates and subduction of oceanic crust* [J]. *Nature communications*, 2021, 12:2534.

<https://doi.org/10.1038/s41467-021-22748-2>

摘要: 大陆是地球所独有的, 并且对大气圈、水圈和生物圈的共同演化发挥着重要作用。然而, 关于大陆的形成和俯冲驱动板块构造的开始存在争议。我们展示了现代和古老的 (4.0-2.8 Ga) 花岗质岩石的 Ca 同位素和微量元素数据以及相平衡模型, 表明 Ca 同位素分馏主要受地温梯度的控制。这些结果要求地温梯度为 500-750°C/GPa, 这与现代 (热) 俯冲带的地温梯度相同, 并与整个太古宙的俯冲活动相一致。然而, 来自加拿大 Nuvvuagittuq Supracrustal Belt 的两个花岗质岩石的地球化学数据不能通过岩浆作用来解释。它们的同位素特征很可能继承自碳酸盐沉积物。这些样品 (> 3.8 Ga) 早于岩石记录中保存的最古老的碳酸盐, 并证实了始太古代海洋中的碳酸盐沉淀为大气 CO₂ 提供了一个重要的汇。结果表明, 俯冲驱动的板块构造作用早在~ 3.8 Ga 之前就开始了。

ABSTRACT: Continents are unique to Earth and played a role in coevolution of the atmosphere, hydrosphere, and biosphere. Debate exists, however, regarding continent formation and the onset of subduction-driven plate tectonics. We present Ca isotope and trace-element data from modern and ancient (4.0 to 2.8 Ga) granitoids and phase equilibrium models indicating that Ca isotope fractionations are dominantly controlled by geothermal gradients. The results require gradients of 500–750 °C/GPa, as found in modern (hot) subduction-zones and consistent with the operation of subduction throughout the Archaean. Two granitoids from the Nuvvuagittuq Supracrustal Belt, Canada, however, cannot be explained through magmatic processes. Their isotopic signatures were likely inherited from carbonate sediments. These samples (> 3.8 Ga) predate the oldest known carbonates preserved in the rock record and confirm that

carbonate precipitation in Eoarchean oceans provided an important sink for atmospheric CO₂. Our results suggest that subduction-driven plate tectonic processes started prior to ~ 3.8 Ga.

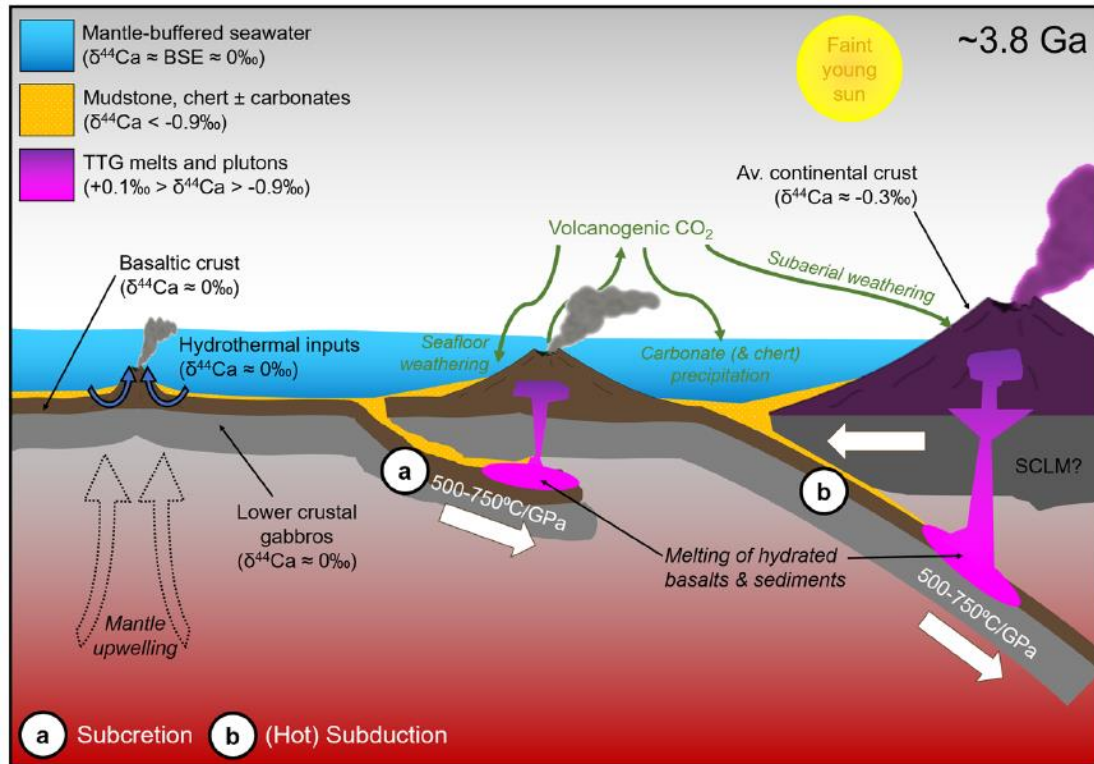
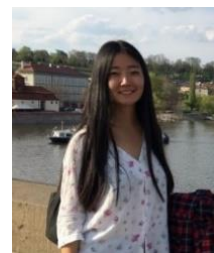


Figure 1. Schematic diagram of geodynamic settings supported by our TTG data [e.g. subcretion (a), localized roll-back (not shown), and/or modernstyle subduction (b)]. Apparent geothermal gradients (500–750°C/GPa) are similar to those reported for modern adakites and hot subduction-zone assemblages. Vigorous hydrothermal circulation promotes mantle-buffered seawater that can lead to isotopically light $\delta^{44}\text{Ca}$ ($< -0.9\text{‰}$) in precipitated carbonates (see Supplementary Note 6), providing a sink for high atmospheric CO₂. Carbonates [along with cherts \pm shales] can then be subducted and incorporated into TTG sources. Av. continental crust average continental crust, BSE bulk-silicate Earth.

3. 冰川-全新世湖泊和陆地环境气候驱动的转变：来自南极东部 Mochou 湖岩石磁学和地球化学证据



翻译人：张琪 zhangq7@sustech.edu.cn

Noronha-D'Mello C, Nair A, Mahesh B, et al. *Glacial-Holocene climate-driven shifts in lacustrine and terrestrial environments: Rock magnetic and geochemical evidence from East Antarctic Mochou Lake [J]. Palaeogeography, Palaeoclimatology, Palaeoecology, 2021, 576: 110505.*

<https://doi.org/10.1016/j.palaeo.2021.110505>

摘要：南极东部冰盖的地貌重建表明，随着气候的变化，冰盖的消退模式具有历时性和多样性。然而，人们对陆地环境如何响应这些气候变化知之甚少，因为大陆冰盖在末次盛冰期（LGM）覆盖了大多数南极洲沿海绿洲，因此消除了陆地记录。本研究，利用地质年代学、岩石学、岩石磁学和地球化学重建了跨越过去 25400 年的环境，以此了解冰期-冰消期气候变化对地表过程和 Mochou 湖生态的影响。在末次冰期（25.4 至 18.8 cal.kyr BP），增强的风力和冰的冻融作用使西部高海拔流域地区风化作用变得活跃，这正是 Mochou 湖沉积物的主要来源。冰川环境条件导致了持续的湖面冰盖，造成缺氧、少量沉淀、初级生产和弱咸性条件。逐渐地，随着公元前 18.8 cal.kyr 左右冰川消退情况的增强，流域融水流量增加，加强了沉积物的运输，并将湖泊转变为一个淡水盆地，尽管常年冰盖仍然普遍存在。此外，与该地区的其他湖泊相比，该湖泊的生物发展始于中全新世，季节性湖泊冰循环和冰壕的形成较晚。响应气候变暖的趋势，流域也开始了较弱的化学风化和成土作用。这种对全新世变暖的延迟响应可能是由于 Dalk 冰川的局部冷却效应，这也导致了 Prydz 湾的海冰持续存在。这项研究还提供了进一步的证据，证明 Larsemann 山的部分地区在末次盛冰期和随后的冰川消退期仍然没有遭到碎冰的侵蚀。特别是 Mirror 半岛，尽管被 Dalk 冰川、Nella 湖冰舌和 Amery 冰架所包围，但还是逃过了冰的覆盖。

ABSTRACT: Geomorphic reconstructions of the East Antarctic Ice Sheet history across Antarctica suggest diachronous and varying retreat patterns with changing climate. However, little is known of how terrestrial environments responded to these

climate changes because the continental ice sheet covered most Antarctic coastal oases during the Last Glacial Maximum (LGM), eliminating terrestrial records. In this study, the environmental history spanning the last 25,400 years was reconstructed using geochronology, lithology, rock magnetism and geochemistry to understand the effect of glacial–deglacial climate variations on surface processes and Mochou Lake ecology. During the last glacial period (25.4 to 18.8 cal. kyr BP), intensified winds and the freeze-thaw action of ice actively weathered the high elevation western catchment that was a dominant sediment source to the lake. The glacial environmental conditions induced a persistent perennial lake ice-cover resulting in anoxia, low sedimentation, primary production and weak brackish conditions. Progressively, as deglacial conditions augmented around 18.8 cal. kyr BP, increased catchment meltwater flow enhanced sediment transport and also transformed the lake into a freshwater basin, although perennial ice-cover still prevailed. Further, the biotic development of the lake began later in the Mid-Holocene as compared to other lakes in the region, wherein the seasonal lake ice cycle and/or ice moat developed. Weak chemical weathering and pedogenesis also commenced in the catchment in response to the warming climate trend. This delayed response to the Holocene warming was possibly due to the local cooling effect of the Dälk Glacier's discharge that also led to sea-ice persistence in the Prydz Bay. This study also provides further evidence that parts of the Larsemann Hills remained free of erosive grounded ice during the LGM and subsequent deglaciation. The Mirror Peninsula, specifically, escaped ice overriding despite being enclosed by the Dälk Glacier, Lake Nella ice lobe and Amery Ice Shelf.

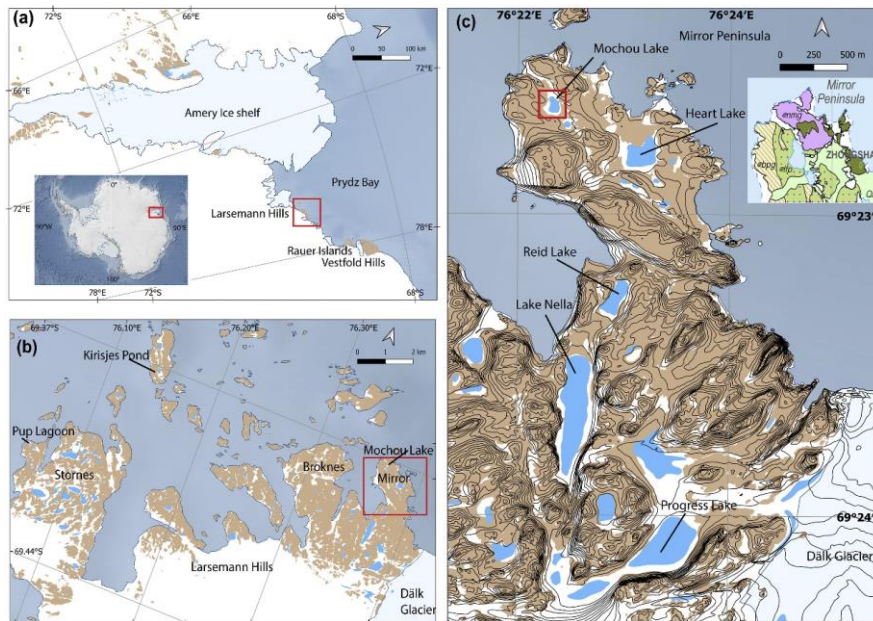


Figure 1. Map showing study area (a) Location of Larsemann Hills in East Antarctica and (b) Mochou Lake at Mirror Peninsula (c) Contour elevation map of Mirror Peninsula (inset) Geology of the study area (Carson and Grew, 2007) with catchment rock type Nella mafic granulite (nmg), Lake Ferris metapelite (lfp), Broknes paragneiss (bpg) and Unconsolidated sediment (Qa).

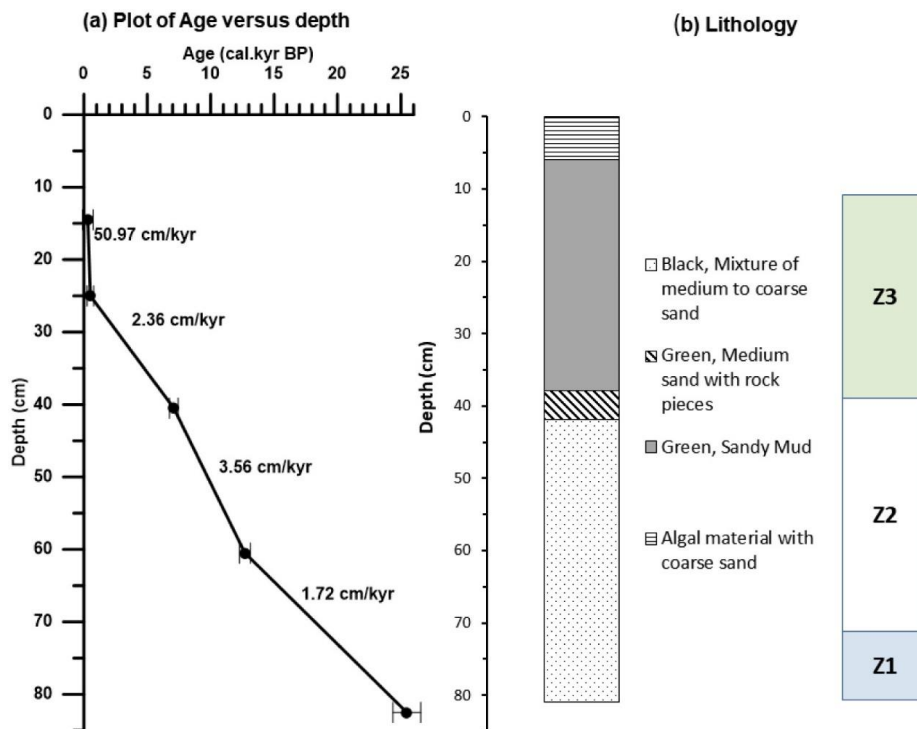


Figure 2. Illustration depicting (a) calibrated ages versus depth with sedimentation rates (cm/kyr) calculated by linear interpolation between two consecutive ages of Mochou Lake core. The derived ages at 0–2 cm and 4–5 cm intervals were not used in the age-depth plot due to reversal of ages in the topmost samples and low reliability. (b) Lake sediment core lithology in zones in Z1, Z2 and Z3.

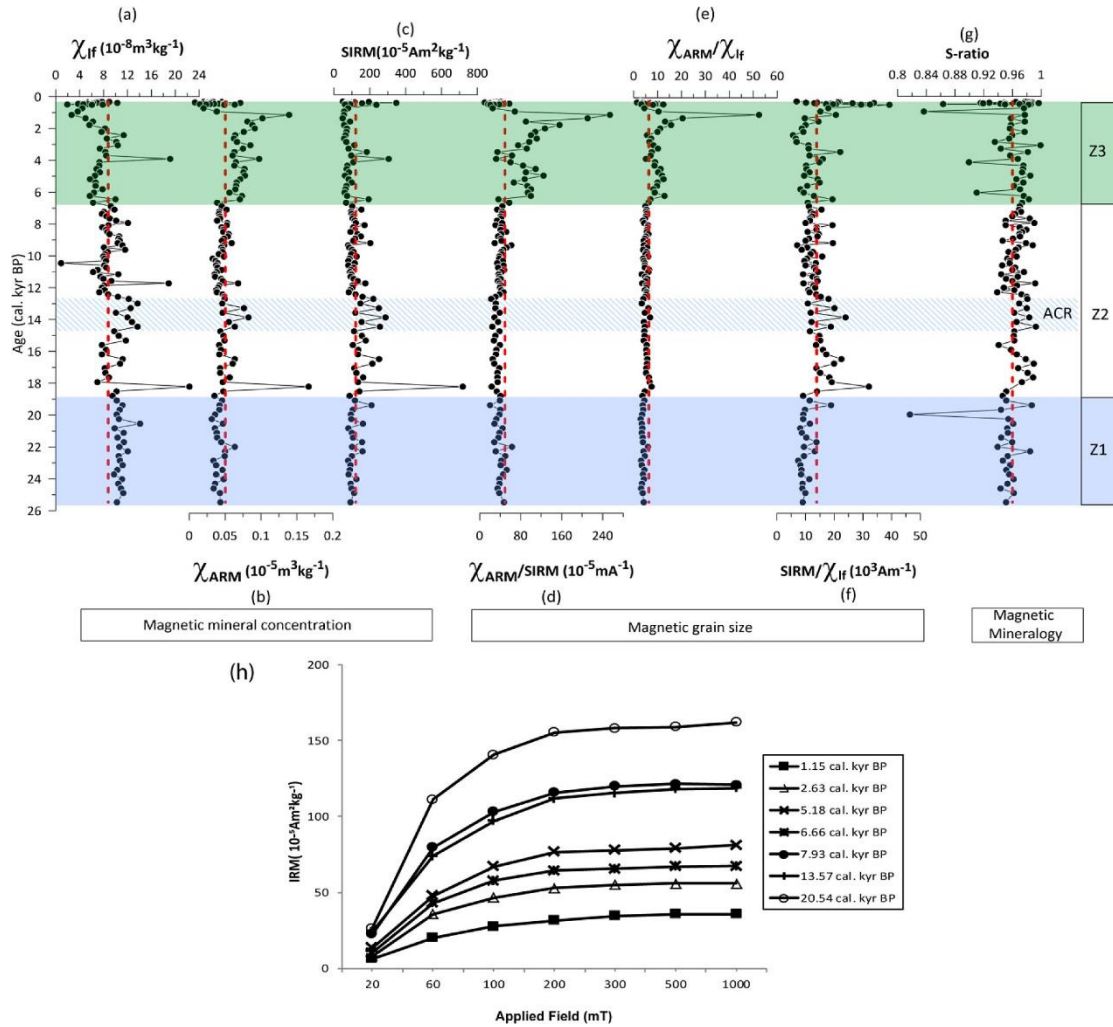


Figure 3. Down-core variations of rock magnetic parameters for the Mochou Lake sediment core (a) Magnetic Susceptibility, (b) Susceptibility of Anhyseric Remanent Magnetization χ_{ARM} (c) Saturated Isothermal Remanent Magnetization SIRM, (d) χ_{ARM}/SIRM , (e) χ_{ARM}/χ_{lf} , (f) SIRM/χ_{lf} (g) S-ratio across -zones Z1 (blue), Z2 (white) and Z3 (green). Patterned band in Z2 represents Antarctic Cold Reversal (ACR). Dashed red line represents the average for respective parameter. (h) Isothermal Remanent Magnetization (IRM) acquisition curves for selected samples of Mochou Lake sediment. (For interpretation of the references to colour in this figure legend, the reader is referred to the web version of this article.)

4. 东南极洲与冈瓦纳曾经相邻的磁场联系

翻译人：曹伟 11930854@qq.com



Ebbing J, Dilixiati Y, Haas P, et al. East Antarctica magnetically linked to its ancient neighbours in Gondwana [J]. Scientific Reports, 2021, 11(1):5513.

<https://doi.org/10.1038/s41598-021-84834-1>

摘要： 本文根据最近的卫星磁场模型（LCS-1）提出了一个新的冈瓦纳中部磁场编译，在等效层方法的帮助下得到同一层位进行校正，并首次进行应用。此外，我们使用卫星数据的全部频谱内容，这有助于包括印度区域信息（那里尚未公开提供高分辨率的航空磁测数据）。由于印度位于磁赤道以北，我们还应用等效源方法对卫星数据进行了动态化极。整合的航磁和卫星数据叠加在最近的可变形冈瓦纳板块重建上，该重建将非洲南部的Kaapvaal克拉通与南极东部的Grunehogna克拉通紧密连接在一起。然而，航磁异常揭示了更广泛的造山带，与南非和印度的相邻地区相比，这些造山带保存了南极东部内陆增生的中新元古代地壳的残余。卫星和航空磁异常数据集有助于描绘早期前寒武纪克拉通的范围和结构，从而加强了它们在南极东部，澳大利亚，印度和非洲的联系。

ABSTRACT: We present a new magnetic compilation for Central Gondwana conformed to a recent satellite magnetic model (LCS-1) with the help of an equivalent layer approach, resulting in consistent levels, corrections that have not previously been applied. Additionally, we use the satellite data to its full spectral content, which helps to include India, where high resolution aeromagnetic data are not publically available. As India is located north of the magnetic equator, we also performed a variable reduction to the pole to the satellite data by applying an equivalent source method. The conformed aeromagnetic and satellite data are superimposed on a recent deformable Gondwana plate reconstruction that links the Kaapvaal Craton in Southern Africa with the Grunehogna Craton in East Antarctica in a tight fit. Aeromagnetic anomalies unveil, however, wider orogenic belts that preserve remnants of accreted Meso-to

Neoproterozoic crust in interior East Antarctica, compared to adjacent sectors of Southern Africa and India. Satellite and aeromagnetic anomaly datasets help to portray the extent and architecture of older Precambrian cratons, re enforcing their linkages in East Antarctica, Australia, India and Africa.

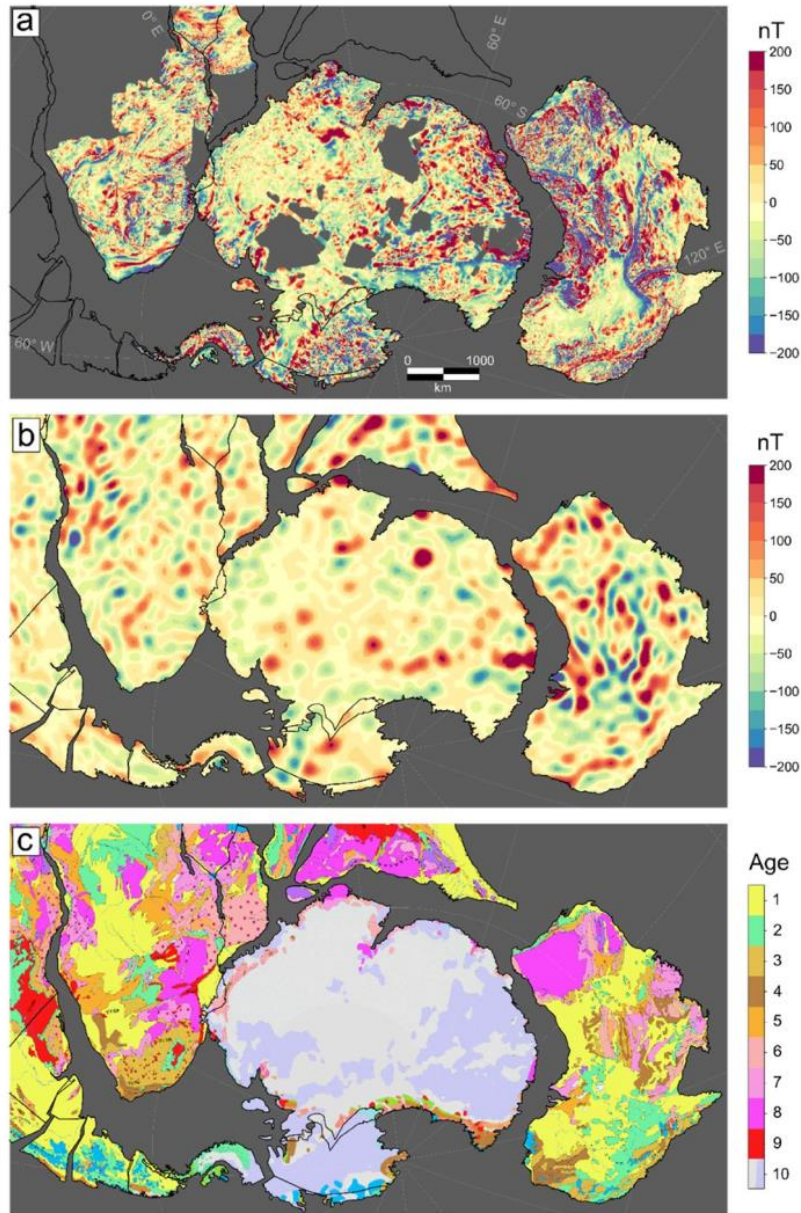


Figure 1. (A) Conformed aeromagnetic data, (B) Satellite model LCS-1 after variable reduction to the pole, represented at 5 km ellipsoidal height. (C) Surface geology as represented in the Geological Map of the World. The geological units are: 1: Cenozoic, 2: Mesozoic, 3: Upper Paleozoic, 4: Lower Paleozoic, 5: Neoproterozoic, 6: Mesoproterozoic, 7: Paleoproterozoic, 8: Archean, 9: Large Igneous Provinces, 10: Glaciers and Ice. All data sets are rotated back to 200 Ma with the deformable plate model.

5. 上新世-更新世过渡时期东赤道太平洋稳定的生物生产力 (3.35-2.0 Ma)

翻译人: 王敦繁 dunfan_w@foxmail.com



Jakob K A, Ho S L, Meckler A N, et al. Stable Biological Production in the Eastern Equatorial Pacific Across the Plio-pleistocene Transition (3.35–2.0Ma) [J]. Paleoceanography and Paleoclimatology, 2021, 36(4): e2020PA003965.

<https://doi.org/10.1029/2020PA003965>

摘要: 在东赤道太平洋(EEP)上升流是影响地球气候的一个关键因素,因为它支持着目前 10%的生物生产力。东太平洋(EEP)上升流在上新世-更新世过渡期间的演化--这段时间对于理解大气二氧化碳变化导致的近期变暖尤为重要--已经在东太平洋上升流区以东地区进行了深入研究。相比之下,在这一海洋屏障以西的开放太平洋中,赤道上升流的变化却明显较少受到关注。因此,我们研究了位于 EEP 大洋上升流区的 IODP 849 站位的古气候记录。我们的目标区间(约 3.35~2.0 Ma)覆盖了以北半球冰川作用加强(iNHG)为特征的上新世-更新世过渡期。我们利用底栖生物 $\delta^{18}\text{O}$ 值为该孔建立了一个新的高分辨率年龄框架,并利用沉积速率和底栖生物 $\delta^{13}\text{C}$ 值来评估净出口生产力。研究表明,虽然显示了暂时性的冰川-间冰期变化,但在整个 iNHG 的长期时间尺度上,净出口生产力是稳定的。我们的研究说明该站位初级生产力的长期演化分以下三个步骤。首先,营养盐从高纬度向 EEP 输出;第二,在该时期太平洋营养线连续浅滩化;第三,同时由粉尘引起的铁输入减少。

ABSTRACT: Upwelling within the Eastern Equatorial Pacific (EEP) Ocean is a key factor for the Earth's climate because it supports >10% of the present-day biological production. The dynamics of upwelling in the EEP across the Plio-Pleistocene transition—an interval particularly relevant for understanding near-future warming due to Anthropocene-like atmospheric carbon-dioxide levels—have been intensively studied for the region east of the East Pacific Rise. In contrast, changes of the equatorial upwelling regime in the open Pacific Ocean west of this oceanographic barrier have

received markedly less attention. We therefore provide new proxy records from Ocean Drilling Program Site 849 located within the EEP open-ocean upwelling regime. Our target interval ($\sim 3.35\text{--}2.0\text{ Ma}$) covers the Plio-Pleistocene transition characterized by the intensification of Northern Hemisphere Glaciation (iNHG). We use benthic $\delta^{18}\text{O}$ values to generate a new, high-resolution age model for Site 849, and sand-accumulation rates together with benthic $\delta^{13}\text{C}$ values to evaluate net export production. Although showing temporary substantial glacial-interglacial variations, our records indicate stability in net export production on secular timescales across the iNHG. We suggest the following processes to have controlled the long-term evolution of primary productivity at Site 849. First, nutrient export from the high latitudes to the EEP; second, a successive shoaling of the Pacific nutricline during the studied interval; and third, a simultaneous reduction in dust-borne iron input.

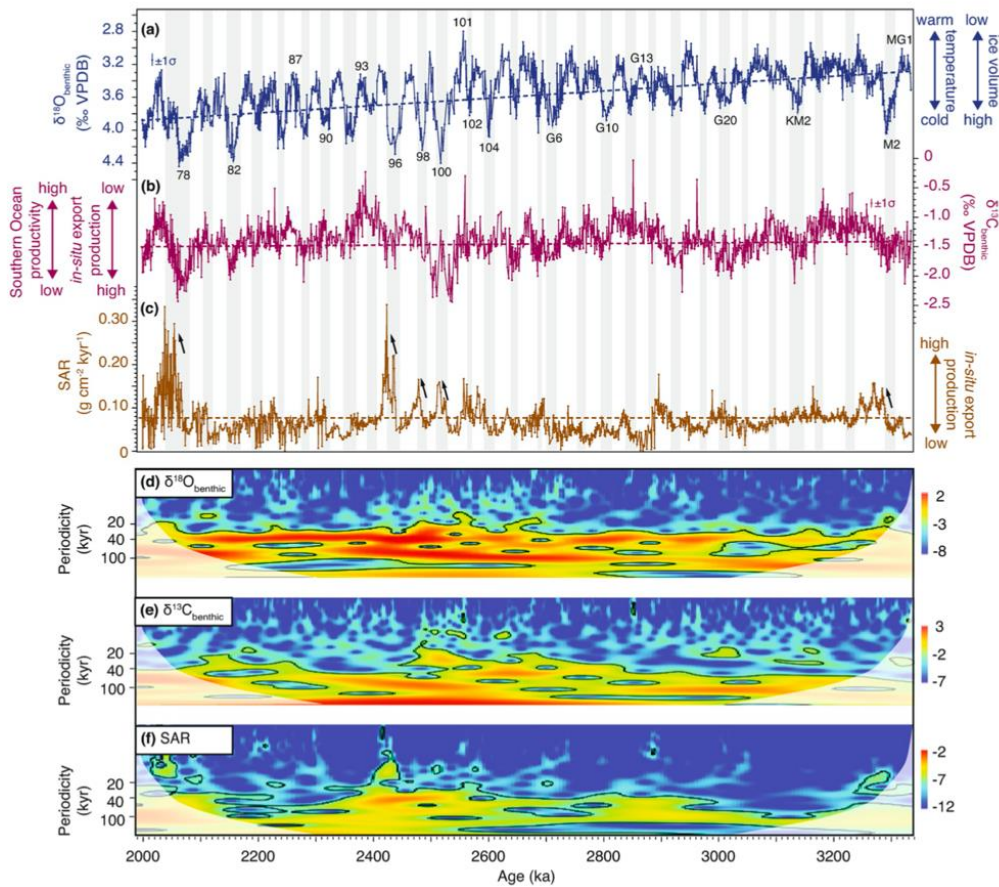


Figure 1. Productivity proxy records for Site 849 for the ~3.35–2.0 Ma interval and evolutionary spectra. (a) Benthic foraminiferal $\delta^{18}\text{O}$ record for reference. (b) Benthic foraminiferal $\delta^{13}\text{C}$ record; high (low) values indicate a mixed signature of low (high) rates of in situ export production but at the same time high (low) rates of primary productivity in EEP source waters. Horizontal and vertical bars in a and b indicate the 1σ standard deviation associated with the individual records. (c) Sand-accumulation rates; high (low) values indicate high (low) rates of in situ export production. Dashed lines in a–c indicate long-term trends and gray bars mark glacial periods; selected MIS are labeled for reference. (d–f) Wavelet analysis for benthic $\delta^{18}\text{O}$, benthic $\delta^{13}\text{C}$ and SAR. Black lines indicate the 95% significance levels; white shading marks the cone of influence, that is the region in which record length might not be sufficient to interpret results.

6. 极弱地磁场的时期延长：埃迪卡拉纪 Grenville(SE Canada) 岩墙的古强度结果

翻译人：张伟杰 12031188@mail.sustech.edu.cn



Thallner D, Biggin A J, Halls H C. An extended period of extremely weak geomagnetic field suggested by palaeointensities from the Ediacaran Grenville dykes (SE Canada) [J]. Earth and Planetary Science Letters, 2021, 568:117025.

<https://doi.org/10.1016/j.epsl.2021.117025>

摘要：在古地磁记录中观察到的地磁场的长期变化，有可能对地球深部的内部演化提供更多的信息。埃迪卡拉纪（635-538 Ma）具有异常方向和超低强度的地磁场特征，是一个特别值得关注的时期。陡或浅的方向，导致虚拟地磁极点（VGPs）分开的角度高达 90°或非常接近，可以记录地磁场轴向和赤道偶极状态之间的转换。也可能，当时的磁场可能只是高度的非偶极子特征或者发生了快速的反转。获得高质量的来自记录着异常方向的地层的古强度结果可能有助于区分古地磁数据的形态与时间变化特征。我们从 Grenville 岩墙群西端的 6 个岩脉中获得了新的古强度，记录了约为 585 Ma 方向异常的地磁场。双加热 Thellier 实验结果未满足数据选择标准，不过从微波 Thellier 方法、Shaw 方法、类 Thellier 方法成功获得了古强度结果，其强度值为 $2.9 \pm 2.2 \mu\text{T}$ 相应的虚偶极矩为 $0.3\text{-}1.7 \times 10^{22} \text{Am}^2$ 。这些磁场强度比现在的地磁场弱一个数量级。分组的 VGP 落在两个明显不同的集合中，但是它们具有一致的角度分散特征（SB=18.5°、18.9°），可能指示着存在赤道偶极子。相反，陡或浅方向的样品获得的古地磁场强度结果没有明显差别。尽管基于较少的结果，整体非常大的 VGP 分散特征可能更支持 Grenville 岩墙记录了与高度不稳定和磁场快速反转相关的长期变化增强的特征。

ABSTRACT: Long-term variations of the geomagnetic field, observed in the palaeomagnetic record, have the potential to shed much light on the evolution of Earth's deep interior. With a geomagnetic field characterised by anomalous directions and ultra-low intensities, the Ediacaran period (635-538 Ma) is a time of special interest. Steep and shallow directions, leading to virtual geomagnetic poles (VGPs) separated by

angles of up to 90° and very close in age could have recorded a geomagnetic field switching between axial and equatorial dipole-dominated states. Alternatively, the field may simply have been highly nondipolar and subject to rapid reversals. Palaeointensity determinations of units that record the anomalous directions could potentially help to discriminate between morphologies but the spatial and temporal distribution of palaeomagnetic data require improvement. Here we present new palaeointensities from 6 dykes from the western end of the Grenville Dyke swarm that recorded directionally anomalous geomagnetic fields around ~ 585 Ma. Results from double-heating Thellier experiments failed to satisfy the used selection criteria, but successful microwave Thellier, Shaw and pseudo-Thellier experiments lead to palaeointensities that show field strength values of $2.9 \pm 2.2 \mu\text{T}$ and corresponding virtual dipole moments of $0.3\text{-}1.7 \times 10^{22} \text{Am}^2$. These field strengths are an order of magnitude weaker than the present-day field. VGPs grouping in two distinct clusters with almost identical angular dispersions of VGPs ($SB=18.5^\circ$ and 18.9°) may argue for the presence of an equatorial dipole. In contrast, the palaeointensities associated with the steep and shallow components are indistinguishable. Although based on a low number of results, this observation, together with the overall very large VGP dispersion may rather support that the Grenville Dykes have recorded enhanced secular variation linked to a highly unstable and rapidly reversing field.

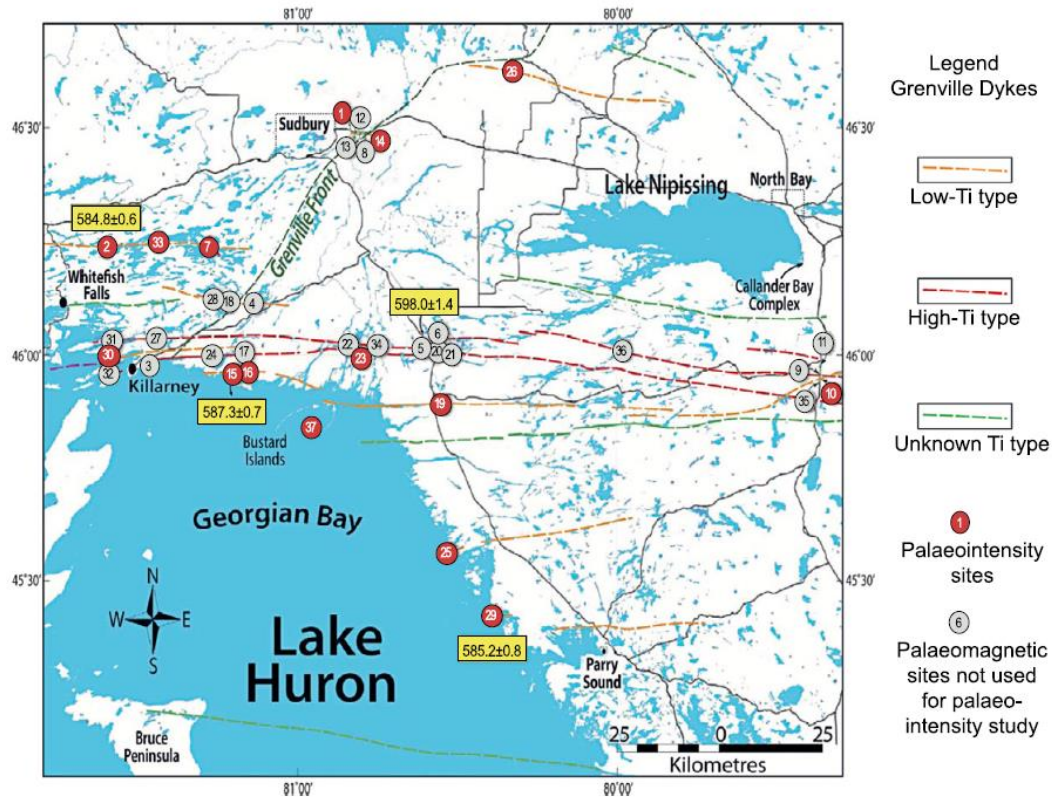


Figure 1. Map of southeast Ontario, showing the Grenville dykes and locations of sites studied in Halls et al. (2015) and sites selected for this palaeointensity study; from Halls et al. (2015). (For interpretation of the colours in the figure(s), the reader is referred to the web version of this article.)

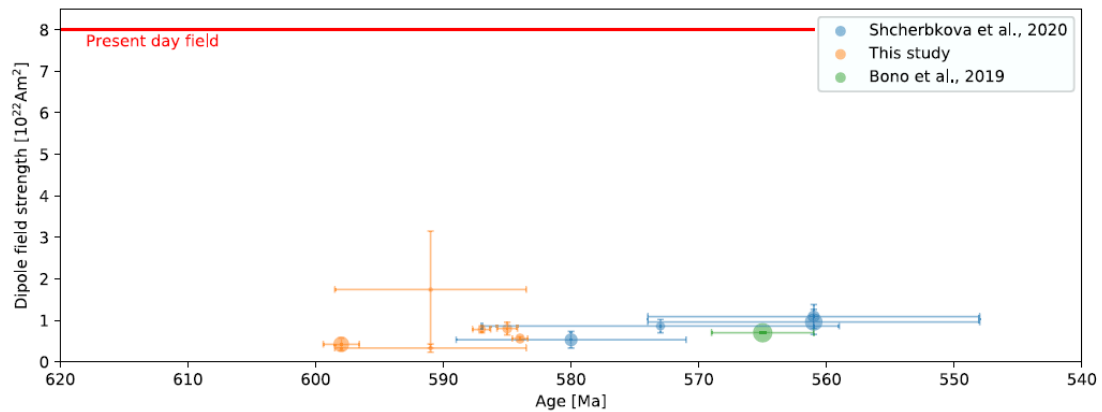


Figure 2. Virtual dipole moments of the Grenville dykes plotted versus age in with virtual dipole moments of the Baltican Volyn traps (Shcherbakova et al., 2020) and the palaeomagnetic dipole moment of the Sept Îles (Bono et al., 2019) in comparison to the present-day field strength. Marker sizes correspond to number of individual intensity estimates N used in the average. Plotted are mean values with $N > 1$. Error bars show estimated age errors and one standard deviation of dipole moments.

7. 末次冰期地磁偶极子场变化—分离气候和生产速率信号后的格陵兰冰芯宇宙核素记录

翻译人：柳加波 liujb@sustech.edu.cn



Zheng M, Sturevik-Storm A, Nilsson A, et al. *Geomagnetic dipole moment variations for the last glacial period inferred from cosmogenic radionuclides in Greenland ice cores via disentangling the climate and production signals [J]. Quaternary Science Reviews, 2021, 258: 106881.*

<https://doi.org/10.1186/s40623-020-01277-0>

摘要：地磁场偶极矩（GDM）通过屏蔽宇宙射线，能够调节宇宙放射性核素的生产速率。因此，利用这种关系，就有可能从冰芯等自然样品中记录的放射性核素来重建 GDM 的变化。基于两根格陵兰冰芯的 ^{10}Be 和 ^{36}Cl 的数据，本文重建了 11.7 ka 至 108 ka b2k（before A.D. 2000）期间的 GDM 变化。我们发现，宇宙核素记录反映了气候和生产速率的共同影响。估算 GDM 的变化则需要分离这些因素的作用。为了最小化与气候相关的同位素变化，我们应用了多线性校正方法，移除了宇宙核素记录中 ^{10}Be 和 ^{36}Cl 和气候参数（累积速率、 $\delta^{18}\text{O}$ 和离子数据）之间的共同变化。获得的“气候校正”过的宇宙核素记录通过理论生成模型转换成 GDM。基于“气候校正”的宇宙核素建立的 GDM 与独立的古地磁方法获得的 GDM 记录具有很好的一致性。此外，与简单的使用宇宙核素通量相比，这种“气候校正”的方法与 GDM 重建具有更好的一致性。这也支持了我们校正方法的有效性，从而将生产速率变化从冰芯宇宙核素记录中分离出来。基于这种校正方法，我们将基于宇宙核素的 GDM 重建延伸至气候信号最强的时期。

ABSTRACT: The geomagnetic dipole moment (GDM) modulates the production rates of cosmogenic radionuclides via the shielding of galactic cosmic rays. Therefore, it is possible to use this linkage to reconstruct past changes in the GDM based on cosmogenic radionuclide records from natural archives such as ice cores. Here we present a GDM reconstruction based on ^{10}Be and ^{36}Cl data from two Greenland ice cores from 11.7 ka to 108 ka b2k (before A.D. 2000). We find that the cosmogenic radionuclide records reflect a mixture of climate and production effects that require

separation to evaluate the changes in the GDM. To minimize climate-related variations on isotope data, we applied a multi-linear correction method by removing common variability between ^{10}Be and ^{36}Cl and climate parameters (accumulation rates, $\delta^{18}\text{O}$ and ion data) from radionuclide records. The resulting “climate corrected” radionuclide data are converted to GDM using a theoretical production model. Comparison of “climate corrected” radionuclides based GDM reconstructions with independent paleomagnetic-derived GDM records shows a good agreement. Furthermore, the “climate correction” leads to an improved agreement with GDM reconstructions than simply using radionuclide fluxes, lending support to the validity of our correction method to isolate production rate changes from ice core radionuclide records. With this correction method, we can extend the GDM reconstructions based on the cosmogenic radionuclides in ice cores to a period when there is a strong climate signal in the data.

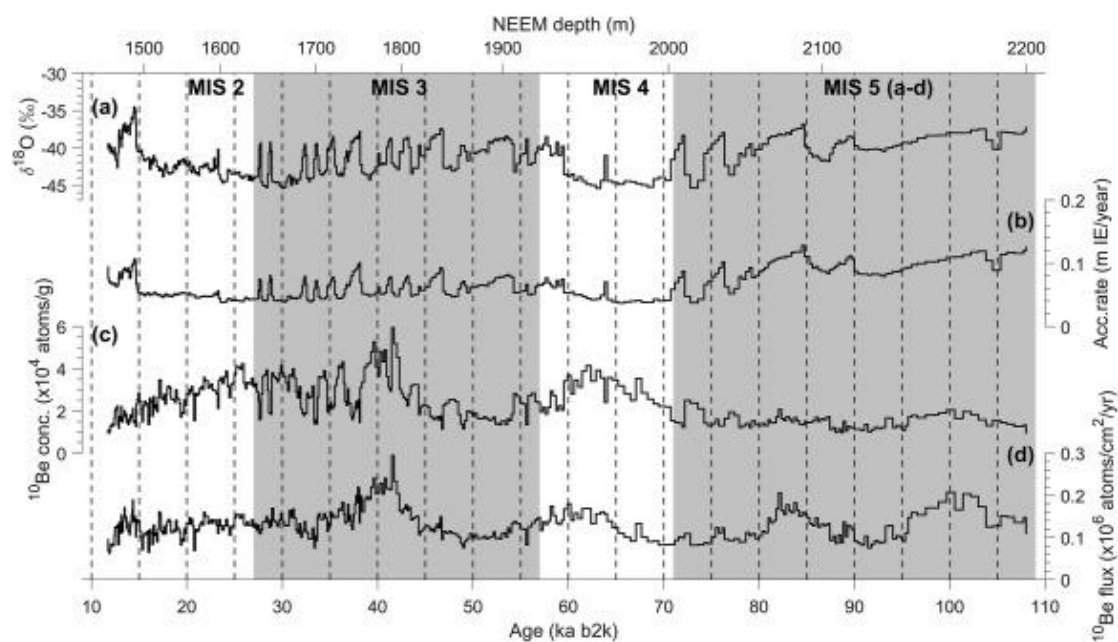


Figure 1. $\delta^{18}\text{O}$, accumulation rates, and ^{10}Be concentrations and fluxes from the NEEM ice core for 11.7–108 ka b2k. (a) NEEM $\delta^{18}\text{O}$ data (NEEM community members, 2013; Schüpbach et al., 2018). (b) NEEM accumulation rates from Rasmussen et al. (2013) averaged four different accumulation reconstructions. (c) NEEM ^{10}Be concentrations. (d) NEEM ^{10}Be fluxes are calculated by multiplying the concentration of each sample with the corresponding accumulation rate and ice density. $\delta^{18}\text{O}$ and accumulation rates are resampled to match the ^{10}Be resolution.

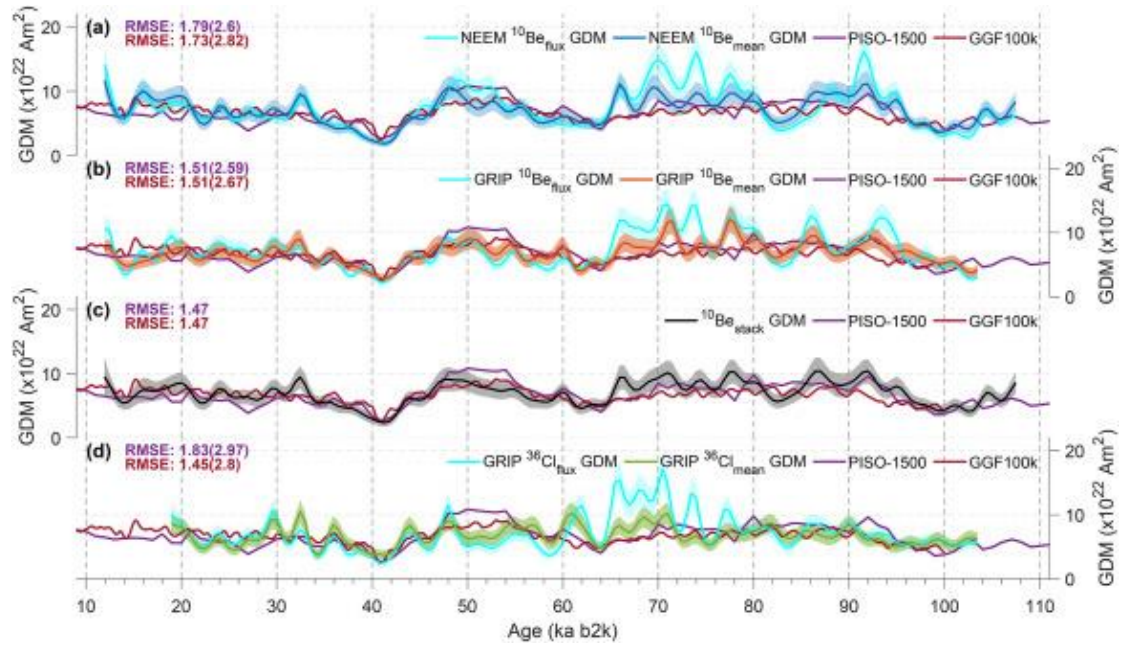


Figure 1. Comparison of $^{10}\text{Be}_{\text{mean}}$ and $^{36}\text{Cl}_{\text{mean}}$ -based GDM reconstructions with the paleomagnetic model reconstruction GGF100k (Panovska et al., 2018b) and the reconstruction from the global relative paleointensity stack PISO-1500 (Channell et al., 2009). The shaded area for the $^{10}\text{Be}_{\text{stack}}$ -based GDM presents its 2 standard error based on bootstrapping from the underlying records and uncertainties in the average GDM. The shaded areas for $^{10}\text{Be}_{\text{mean}}$ -, $^{36}\text{Cl}_{\text{mean}}$ -, $^{10}\text{Be}_{\text{flux}}$ -, and $^{36}\text{Cl}_{\text{flux}}$ -based GDM only indicate the uncertainties based on different assumed average GDM. The RMSE (Root Mean Square Error) values in the bracket are the ones between uncorrected $^{10}\text{Be}_{\text{flux}}$ - and $^{36}\text{Cl}_{\text{flux}}$ -based GDM reconstructions and PISO-1500 and GGF100k.

8. 由希克苏鲁伯撞击触发的显著而短暂的海洋生产力爆发



翻译人: 蒋晓东 jiangxd@sustech.edu.cn

Brugger J, Feulner G, Hofmann M, et al. A pronounced spike in ocean productivity triggered by the Chicxulub impact [J]. Geophysical Research Letters, 2021, 48:e2020GL092260.

<https://doi.org/10.1029/2020GL092260>

摘要: 越来越多的证据表明白垩纪-第三纪分界的生物大灭绝是由墨西哥希克苏鲁伯附近的小行星撞击引起。本研究通过模型模拟探究了硫酸盐气溶胶、二氧化碳、粉尘在撞击初期及之后对大洋环境以及海洋生物圈的影响。我们发现撞击发生后出现了强烈的温度降低和短暂的藻类爆发,这是由深海翻涌和海表酸化提供了营养物质。将模型指示的撞击后变暖和碳同位素的变化与实验证据相比较,结果表明陆地生物圈释放了大量的碳。总之我们的结果阐明了希克苏鲁伯小行星撞击后几十年至几百年时间段内的环境变化,这些变化是很难用指标性数据说清楚。

ABSTRACT: There is increasing evidence linking the mass-extinction event at the Cretaceous-Paleogene boundary to an asteroid impact near Chicxulub, Mexico. Here we use model simulations to explore the combined effect of sulfate aerosols, carbon dioxide and dust from the impact on the oceans and the marine biosphere in the immediate aftermath of the impact. We find a strong temperature decrease, a brief algal bloom caused by nutrients from both the deep ocean and the projectile, and moderate surface ocean acidification. Comparing the modeled longer-term post-impact warming and changes in carbon isotopes with empirical evidence points to a substantial release of carbon from the terrestrial biosphere. Overall, our results shed light on the decades to centuries after the Chicxulub impact which are difficult to resolve with proxy data.

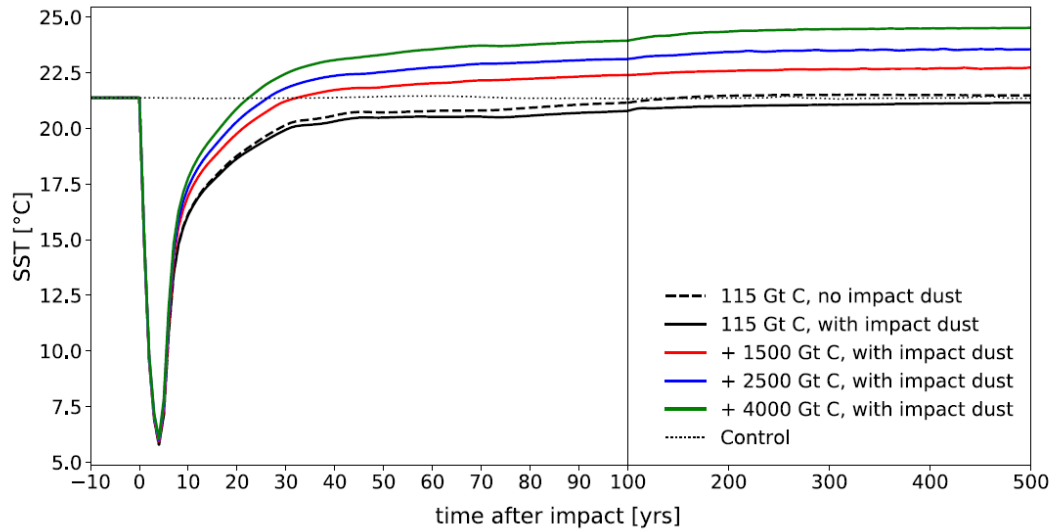


Figure 1. Sea surface temperature evolution for different amounts of carbon released due to the impact. Annual and global mean sea surface temperature before and after the impact for simulations with (solid lines) and without the effects of dust produced during the impact (dashed line) as well as for different amounts of organic carbon released from terrestrial reservoirs (colored lines).

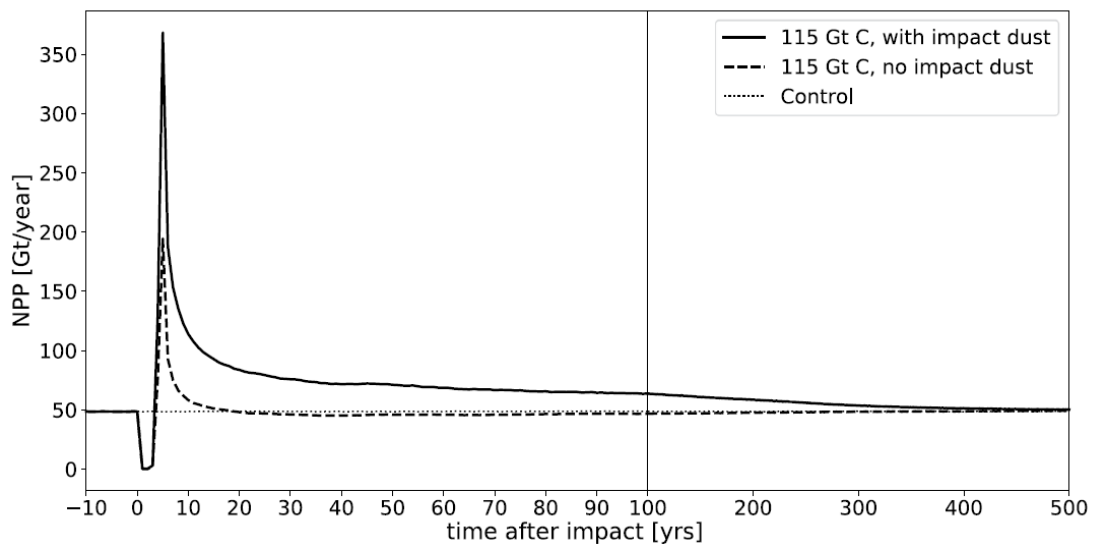


Figure 2. Effects of the impact on the marine biosphere. Annual and global mean ocean net primary productivity before and after.

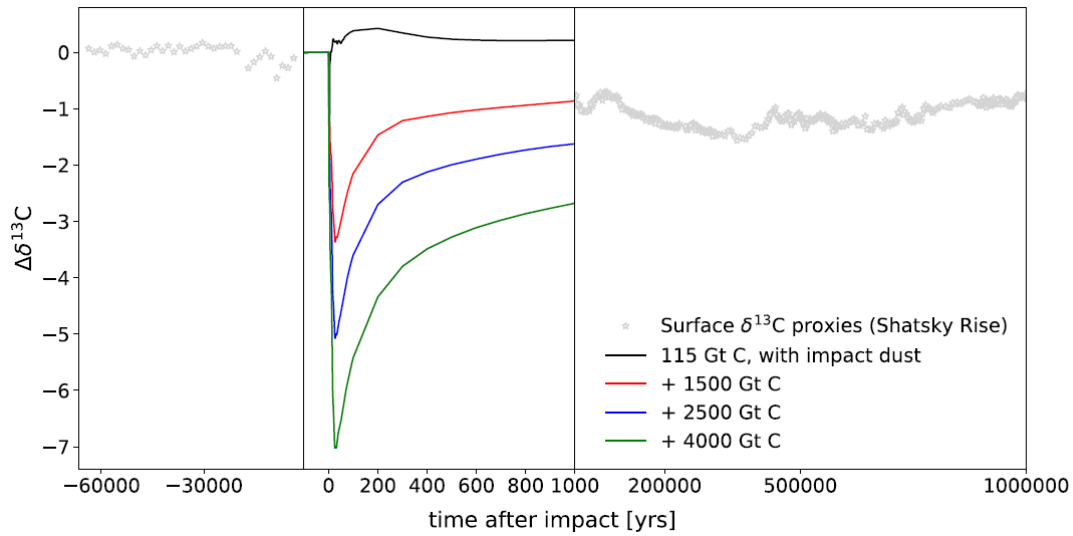


Figure 3. Changes of surface carbon isotope ratios of dissolved inorganic carbon at Shatsky Rise, Pacific. Colored lines show modeled changes in $\delta^{13}\text{C}$ for the 1,000 years after the impact relative to the 100-year pre-impact mean for simulations with different amounts of carbon. The model results are embedded in changes in surface $\delta^{13}\text{C}$ from proxy data from bulk carbonate (Table S11 in Hull et al., 2020), assuming an absolute age for the K-Pg boundary of 66.022 Ma (Table S3 in Hull et al., 2020) relative to the mean of the pre-impact proxy values.

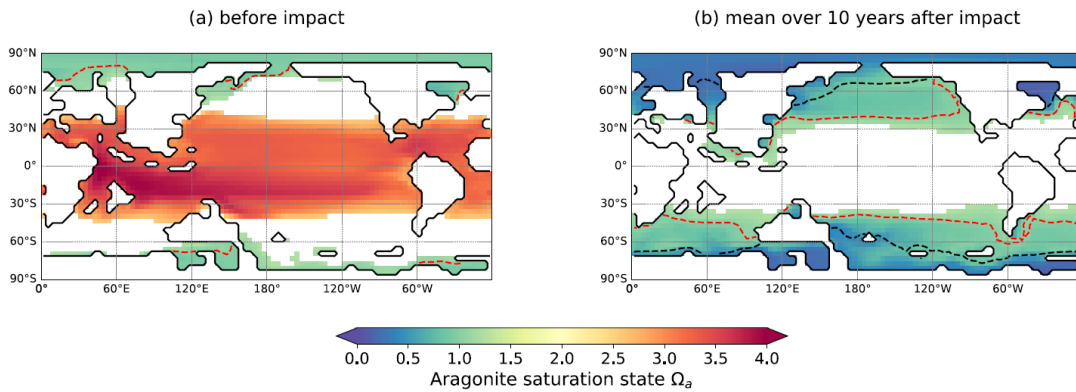


Figure 4. Effects of carbon and sulfur emissions from the impact on ocean acidification. Surface ocean aragonite saturation state before the impact (a) and for the average over the 10 years after the impact. The $\Omega_a = 1$ line is shown in red. The dashed black line in (b) shows $\Omega_a = 1$ for the 1,000 years after the impact.